Direct Observation of Pinning and Bowing of a Single Ferroelectric Domain Wall

T. J. Yang,[1] Venkatraman Gopalan,[2] P. J. Swart,[3] and U. Mohideen[1,*]

[1]*Department of Physics, University of California, Riverside, California 92521*
[2]*Department of Materials Science and Engineering, The Pennsylvania State University, University Park, Pennsylvania 16802*
[3]*Theoretical Division, Los Alamos National Laboratory, Los Alamos, New Mexico 87545*
(Received 19 November 1998)

We have made a direct optical observation of pinning and bowing of a single 180° ferroelectric domain wall under a uniform applied electric field using a collection mode near-field scanning optical microscope. The domain wall is observed to curve between the pinning defects, with a radius of curvature determined by the material parameters and the applied electric field. The change in birefringence with applied field is used to infer the orientation of the internal field at the domain wall. [S0031-9007(99)09111-5]

PACS numbers: 77.80.Dj, 61.16.Ch

Domain wall movement plays a key role in the macroscopic response of ferroelectrics, ferromagnets, and ferroelastics [1]. In particular, the pinning-depinning dynamics caused by randomly distributed defects and impurities is of great interest, since it not only provides fundamental insight into the physics of driven disordered systems, but is also of technological relevance (e.g., in ferromagnetic and ferroelectric based memory devices). In these materials, domain wall movement can result in a complex nonlinear macroscopic response, displaying significant hysteresis and slow aging. While the control and manipulation of pinning is central to enhancing properties, there is very little microscopic and detailed information of domain wall movement under applied fields. Here, we have used a polarization sensitive collection mode near-field scanning optical microscope (CMNSOM) [2] to perform direct submicroscopic investigations of domain wall movement, pinning, and bowing under a uniform applied field. We observe that domain wall motion is possible for fields only a tenth of the coercive field. This motion is the submicroscopic bending of the domain wall between pinning sites. This provides direct evidence that coercive fields reported for many ferroelectrics may correspond to a pinning-depinning transition of domain walls [3].

A variety of experimental techniques such as polarizing optical microscopy, etching, colloidal decoration, the anomalous dispersion of x rays, scanning force microscopy, scanning electron microscopy, and transmission electron microscopy have been used to study static domains [3–7]. The CMNSOM [2,8] with a spatial resolution around a fifth of an optical wavelength is ideally suited for studying domain walls under uniform applied fields. A schematic of the experimental setup is shown in Fig. 1. Here, light transmitted through the crystal is collected with an aluminum coated fiber probe (aperture <100 nm and maintained <5 nm from the surface) and its polarization rotation is measured.

The experiments were performed on the room temperature $3m$ ferroelectric phase of $LiTaO_3$. Single domain crystals cut perpendicular to the c axis (spontaneous polarization axis) and of 0.5 mm thickness were used. Crystal surfaces of optical polish were used. The lithium deficiency in these congruent crystals (Li/[Li + Ta] $\sim$ 0.485) results in large internal fields of order $\sim$5 kV/mm through point defect complexes. In the original single domain crystal, the internal field from the chemical impurities is oriented parallel to the spontaneous polarization direction through a poling process done at 600 °C. Crystal defects such as dislocations (fewer in number) have randomly oriented internal fields. Then 180° domains are created at room temperature with an external electric field. This room temperature process leaves the internal field due to the chemical impurities unchanged [9]. Therefore, across domain walls studied here, while the spontaneous polarization rotates by 180°, the orientation of the internal field due to the chemical defects remains the same [9]. A 20 nm semitransparent 60% Au + 40% Pd electrode
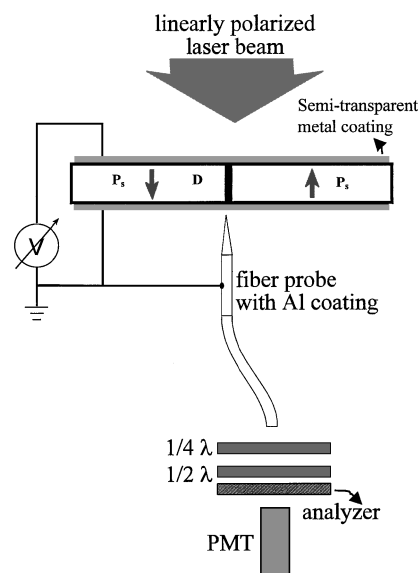

FIG. 1. Experimental schematic of electroded $LiTaO_3$ crystal with the 180° domain wall (D), associated spontaneous polarization (P_s), quarter ($\lambda/4$) and half ($\lambda/2$) wave plates.

    0031-9007/99/82(20)/4106(4)\$15.00

was sputtered on the top and bottom surfaces of the crystal. The bottom electrode and fiber probe are grounded. Both positive and negative voltages are applied to the top electrode.

In the experiment, the fiber probe is first placed and maintained in the near field (<5 nm) of the crystal surface using the shear force technique [2]. Linear polarized light from an argon ion laser is passed through a half-wave plate (to change incident polarization) and is incident normally on the top surface of the crystal. The transmitted light collected by the fiber probe at the bottom surface is collimated and passed through a half-wave plate and quarter-wave plate which are set to compensate for fiber birefringence. The light is then passed through an analyzer and is collected by a cooled photomultiplier tube (PMT). At the start of the scan, the analyzer is rotated to null the transmitted light in a region away from the domain wall (region of isotropic refractive index). The background signal under crossed polarizers is measured and subtracted from all images. A 13×13 μm scan of the crystal surface around the birefringent domain wall is then made.

The intensity I transmitted through the analyzer to first order is (the background subtraction above takes care of oblique coupling of scattered light into the probe) [8]

$$I = I_0[\sin^2\phi \sin^2\theta + \cos^2\phi \cos^2\theta$$
$$+ \tfrac{1}{2}\sin(2\phi)\sin(2\theta)\cos(\Delta nkl)]. \qquad (1)$$

Here, Δn is the difference in refractive index (birefringence) between axes parallel and perpendicular to the domain wall, k is the propagation vector for light in the crystal, and l is the crystal thickness. I_0 is the intensity detected through the fiber in an isotropic region of the crystal and is proportional to the incident intensity on the top surface of the crystal. Also, ϕ is the angle of incident polarization, and θ is the analyzer direction, measured with respect to the domain wall. Use of Eq. (1), for a given θ and ϕ, and the measured I at an isotropic region ($\Delta n = 0$) will yield the incident intensity I_0. The measured I at the domain wall for the associated θ and ϕ is used to calculate Δn. The various ϕ and θ are used to make a consistent measurement of Δn.

Figure 2(a) is a single 180° domain wall observed with both electrodes grounded. The incident light polarization was 70° to the domain wall. The FWHM of the birefringent region is 3 μm. The large width of the birefringence is due to internal fields generated by defects pinning the domain wall. The width of the birefringent region in these samples range from less than 100 nm (instrument resolution limit) to a few microns [8]. Given that the metal electrodes used do not have complete transmission and that
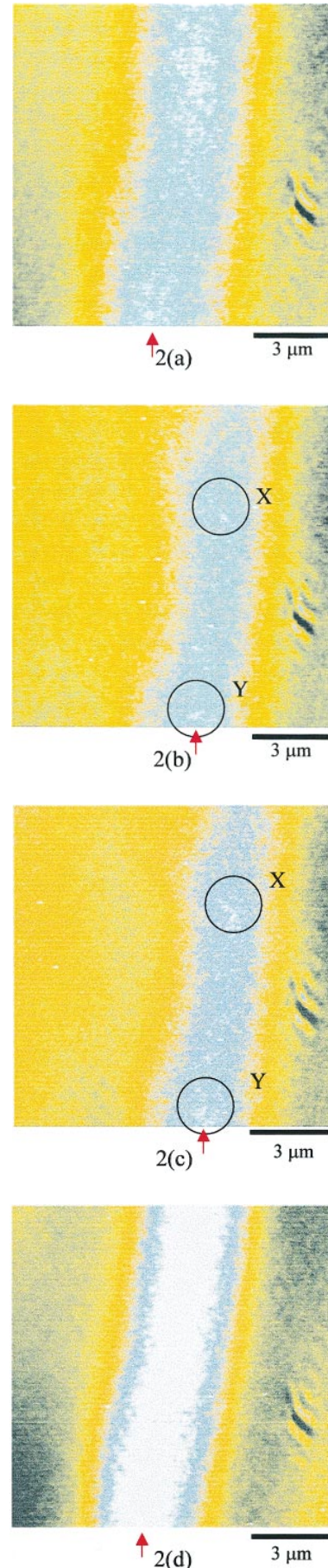

FIG. 2(color). CMNSOM optical signal around the 180° domain wall at applied fields of (a) 0, (b) $+1.5$ kV/mm, (c) $+2.0$ kV/mm, and (d) -1.8 kV/mm. The arrow identifies the bottom of the domain wall. The open circles X and Y in (b) and (c) identify pinning defects from the increased birefringence (brightness) and curvature of the domain wall.

pinning was the object of this study, only domain walls with large birefringence were studied. The dark feature 1.0 μm from the right and 5 μm from the bottom is due to a defect in the electrode which can be used as a position reference. From the reproducibility of optical features on repeated scans of the same region, we estimate the resolution to be of order 150 nm. Next, voltages in steps of $+100$ V are applied to the top electrode. Figure 2(b) shows the optical signal corresponding to the domain wall at an applied field of $+1.5$ kV/mm. The bottom of the domain wall (shown by arrow) is observed to have moved a distance of 3 μm. Figure 2(c) is the optical signal at an applied electric field of $+2$ kV/mm. From Figs. 2(b) and 2(c), we observe that the domain wall has not moved but appears to be pinned at two points (shown by open circles X and Y). The pinning points are identified by their increased birefringence and the change in curvature of the domain wall around them. The exact nature of these pinning defects is not known at present, but they are thought to be physical defects such as screw dislocations or localized variations of point defects [10]. The increased birefringence at the pinning defects results from the associated fields and strains of these defects. Such bending of the domain walls around pinning defects has been predicted in ferroic materials [11]. Next, the applied voltages on the top electrode are brought to zero, and the domain wall was found to relax back to its original position as in Fig. 2(a). Then negative voltages in steps of -100 V are applied to the top electrode. The domain wall at an applied electric field of -1.8 kV/mm is shown in Fig. 2(d). Comparing to Fig. 2(a), no movement of the domain wall is observed. Instead the birefringence

(width and magnitude) at the domain wall was observed to increase with increasing magnitude of the applied field. This asymmetry in domain wall motion with voltage polarity is consistent with the internal electric field orientation which is parallel (antiparallel) to the spontaneous polarization to the left (right) of the domain wall. This is consistent with measurements in Ref. [9] where a coercive field of 21 kV/mm (11 kV/mm) for domain movement to left (right) was found for similar samples.

From the profile of the pinned domain wall in Figs. 2(b) and 2(c), we approximately estimate the domain wall energy based on a simple 2D model shown in Fig. 3 (a detailed analysis based on the Landau theory will appear elsewhere). Let $y = g(x)$ represent a domain wall between two pinning sites $P_1(0,0)$ and $P_2(d,0)$ such that $g(0,0) = g(d,0) = 0$. Under an externally applied field E, the free energy change (ΔU) per unit thickness associated with the domain wall is

$$\Delta U[g] = -2 \cdot P_s E \int_0^d g(x)\, dx$$
$$+ \sigma_w \int_0^d \sqrt{1 + \left(\frac{\partial g(x)}{\partial x}\right)^2}\, dx,$$

where P_s is the spontaneous polarization and σ_w is the domain wall energy per unit area. The depolarization energy and the anisotropic elastic coupling are neglected in this 2D model. The first term is the lowering of the electrostatic free energy by bending of the domain wall, and the second term is the increase in free energy due to increased wall length. For a material (constant P_s) at electric field E, the shape is given by the Euler-Lagrange equation:

$$g(x) = \pm \left\{ \sqrt{\left(\frac{\sigma_w}{2P_s E}\right)^2 - \left(x - \frac{d}{2}\right)^2} - \sqrt{\left(\frac{\sigma_w}{2P_s E}\right)^2 - \left(\frac{d}{2}\right)^2} \right\}.$$

Hence, $g(x)$ is the circle segment of radius $R = \sigma_w/(2P_s E)$, and the domain wall curvature is unique for a given material at a fixed electric field E, independent of the distance between pinning sites. From the profile of the domain wall between the pinning sites in Fig. 2(c), we measure the radius of curvature to be between 6–12 μm (inexactness due to the diffuse nature

of the left edge) giving a domain wall energy per unit area of $\sigma_w = 0.2$–0.4 J/m^2.

Another method of estimating domain wall energy is from the birefringence which results from strain through the photoelastic effect and the internal electric field through the electro-optic effect [8]. Given $3m$ crystal symmetry, the change in refractive index (keeping terms quadratic in the electric field) is

$$\frac{2\Delta n}{n_1^3} = \{2p_{14}d_{15} - 2d_{22}(p_{11} - p_{12}) - 2r_{22}\}E_2 + \{(p_{11} - p_{12})(\gamma_{12} - \gamma_{11}) - 2\gamma_{14}p_{14} + (K_{12} - K_{11})\}(E_2^2 - E_1^2)$$
$$+ \{4(p_{11} - p_{12})\gamma_{41} + 4p_{14}\gamma_{44} + 4K_{14}\}E_2E_3. \tag{2}$$

With reference to Fig. 2(a), x_1 (x_2) is parallel (perpendicular) to the domain wall while x_3 is normal to the plane of the figure. The p_{ij} are photoelastic constants, r_{ij} are linear electro-optic constants, E_k are electric fields, and K_{ilm} are the quadratic electro-optic constants. In Eq. (2), strains ε_j are replaced by $\varepsilon_j = d_{mj}E_m + \gamma_{ilj}E_iE_l$, where d_{mj} are the piezoelectric constants, and γ_{ilj} are the electrostrictive

constants. The bulk material constants [12] can be used due to the small value of strain. The average measured value of birefringence for the domain wall shown in Fig. 2(a) is 1.2×10^{-4}. If we neglect the electrostrictive and quadratic electro-optic terms in Eq. (2) (contribution $<10\%$), the internal electric field across the domain wall $E_2 = 20$ kV/mm. The energy per unit area due to E_2 is
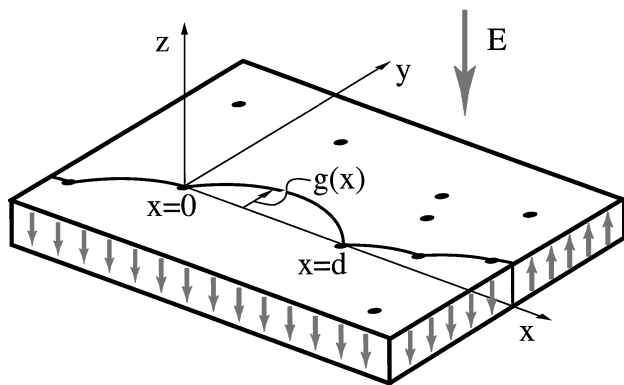
FIG. 3. Schematic of bowing of a pinned domain wall (defects are dots) under an applied electric field.

$w\kappa_2\varepsilon_0 E_2^2/2 = 0.24$ J/m^2, where $w = 3$ μm is the width of the birefringent region at the domain wall, and $\kappa_2 = 45$ is the dielectric constant in the x_2 direction. Given that $E_2 \gg E_1, E_3$ [8] and that the electrostatic energy $\gg$ strain energy [8], the domain wall energy $\sigma_w \sim 0.24$ J/m^2 is consistent with the value calculated from Fig. 3. This domain wall energy is at the high end of some theoretical estimates, e.g., 0.1–0.01 J/m^2 for BaTiO$_3$ [13].

The orientation of the internal electric field in the x_3 direction and second order contributions to birefringence can be inferred by applying negative voltages to the top electrode. In Fig. 4, the solid squares are the average birefringence measured at the domain wall for four different negative voltages and the solid line is a linear least squares fit. The linear increase of the birefringence with applied field in Fig. 4 is to be expected from Eq. (2) as $E_3 = E_3^{\text{internal}} + E_3^{\text{applied}}$. Here the "+" sign is used as the applied field leads to an increase in birefringence (applied field in same direction as internal field), and E_2 is assumed constant as the domain wall remains fixed and $E_2 \gg E_3$ [8]. In Eq. (2), the slope $\frac{n_1^3 E_2}{2}\{4(p_{11} - p_{12})\gamma_{41} + 4p_{14}\gamma_{44} + 4K_{14}\}$ of the line in Fig. 4 is 10^{-11},
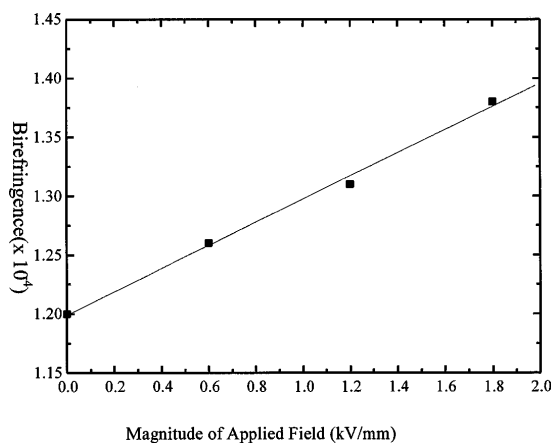

FIG. 4. The birefringence (solid squares) plotted as a function of the magnitude of the applied field. The solid line is the best fit to the data.

leading to $K_{14} = 2 \times 10^{-20}$ m^2/V^2 which is in the correct range between 0.2–2×10^{-20} for quadratic electro-optic coefficients in LiTaO$_3$ [12].

In conclusion, we report a direct measurement of pinning, movement, and profile of a single 180° domain wall under uniform applied fields in single crystals using a CMNSOM. Domain wall birefringence is used in the detection. Fields a tenth of the coercive field are found to move the domain wall. The domain wall is pinned by subsurface defects, which could be identified from the increased birefringence and the profile of the domain wall. The radius of curvature of the pinned domain wall is determined by material parameters and applied electric field. From the profile of the domain wall between the pinning defects, we estimate the domain wall energy between 0.2–0.4 J/m^2. This value of the domain wall energy is consistent with that measured from birefringence at the domain wall. The change in birefringence with applied field of the pinned domain wall is related to the quadratic electro-optic and electrostrictive effect and is used to infer the direction of the internal field.

*To whom correspondence should be addressed.
Email address: umar.mohideen@ucr.edu

[1] A. Hubert and R. Schafer, *Magnetic Domains: the Analysis of Microstructures* (Springer-Verlag, Heidelberg, 1998); E. K. H. Salje, *Phase Transitions in Ferroelastic and Co-elastic Crystals* (Cambridge University, Cambridge, England, 1990).

[2] E. Betzig and J. K. Trautman, Science **257**, 189 (1992); D. W. Pohl and D. Courjon, *Near-Field Optics* (Kluwer Academic Publishers, Karlsruhe, Germany, 1993).

[3] V. Gopalan, T. E. Mitchell, and K. E. Sickafus, Solid State Commun. **109**, 111 (1999).

[4] J. Kobayashi, Phys. Status Solidi **21**, 151 (1967).

[5] F. Saurenbach and B. D. Terris, Appl. Phys. Lett. **56**, 1703 (1990); O. Kolosov *et al.,* Phys. Rev. Lett. **74**, 4309 (1995); L. M. Eng *et al.,* Ferroelectrics **186**, 49 (1996).

[6] S. Stemmer *et al.,* Philos. Mag. A **71**, 713 (1995).

[7] S. Zhu and W. Cao, Phys. Rev. Lett. **79**, 2558 (1997).

[8] T. J. Yang and U. Mohideen, Phys. Lett. A **250**, 205 (1998).

[9] V. Gopalan and M. C. Gupta, J. Appl. Phys. **80**, 6099 (1996); Appl. Phys. Lett. **68**, 888 (1996); K. Kitamura *et al.,* Appl. Phys. Lett. **73**, 3073 (1998).

[10] J. D. Venables, Appl. Phys. Lett. **25**, 254 (1974).

[11] E. K. H. Salje and Y. Ishibashi, J. Phys. Condens. Matter **8**, 8477 (1996).

[12] K. H. Hellwege, in *Crystal and Solid State Physics,* edited by T. Mitsui and S. Nomura, Landolt-Bornstein, New Series, Group III, Vol. 16 (Springer-Verlag, Berlin, 1981).

[13] J. Padilla *et al.,* Phys. Rev. B **53**, R5969 (1996); R. E. Loge and Z. Suo, Acta Mater. **44**, 3429 (1996).